ENVIRONMENTAL RESEARCH
LETTERS

LETTER • OPEN ACCESS

Contrasting responses of the ocean's oxygen minimum zones to artificial re-oxygenation

View the article online for updates and enhancements.

ENVIRONMENTAL RESEARCH
LETTERS

CrossMark

LETTER

Contrasting responses of the ocean's oxygen minimum zones to artificial re-oxygenation

Houda Beghoura[1,*] (iD), Thomas Gorgues[1], Filippa Fransner[2] (iD), Pierre-Amaël Auger[1] (iD) and Laurent Memery[3]

[1] Univ Brest, CNRS, Ifremer, IRD, Laboratoire d'Océanographie Physique et Spatiale (LOPS), IUEM, F29280 Plouzané, France
[2] Geophysical Institute, University of Bergen, and Bjerknes Centre for Climate Research, Bergen, Norway
[3] Laboratoire des Sciences de l'Environnement Marin (LEMAR), UBO/CNRS/IRD/Ifremer, Institut Universitaire Europeén de la Mer (IUEM), Plouzané, France
* Author to whom any correspondence should be addressed.

E-mail: houda.beghoura92@gmail.com

Abstract

Studies assessing potential measures to counteract the marine deoxygenation attributed to anthropogenic activities have been conducted in a few coastal environments and at regional scale, but not yet on a global scale. One way toward global scale artificial oxygenation would be to use oxygen produced as a by-product from hydrogen-production through electrolysis. The low-carbon footprint renewable production of hydrogen from offshore wind energy offers such a possibility. Here, we assessed the potential of this artificial oxygenation method on a global scale using a coupled physical-biogeochemical numerical model. The anthropogenic oxygen source scenario assumes worldwide adoption of hydrogen, considering demographic changes and the feasibility of offshore wind turbine deployment. Following this scenario, artificial oxygenation had a negligible effect on the overall oxygen inventory (an increase of 0.07%) but showed a reduction in the overall volume of Oxygen Minimum Zones (OMZs) between 1.1% and 2.4%. Despite the decrease in the mean OMZ volume globally, OMZs display distinct and contrasting regional patterns notably due to the oxygen impacts on the nitrogen cycle. Artificial oxygenation can inhibit denitrification resulting in a net gain of nitrate that promotes locally and remotely increased biological productivity and consequent respiration. Increased respiration could ultimately lead to an oxygen loss at and beyond injection sites as in the Tropical Pacific and Indian Ocean and particularly expand the Bay of Bengal OMZ. In contrast, the tropical OMZ shrinkage in the Atlantic Ocean is attributed to oxygen enrichment induced by advective transport into the OMZ, while the absence of denitrification in this area precludes any biochemical feedback effect on oxygen levels. These results suggest that the impacts of artificial oxygenation on oxygen concentrations and ecosystems are highly non-linear. It can produce unexpected regional responses that can occur beyond the injection sites which make them difficult to forecast.

1. Introduction

Oxygen availability is important to marine ecosystems notably because of its control on biological respiration and organic matter (OM) remineralization. The dissolved oxygen (O_2) supply to the ocean occurs through atmospheric air–sea gas exchange and release from photosynthesis [1]. While oxygen is abundant in the upper ocean, vast zones of the ocean display naturally low oxygen concentrations known as Oxygen Minimum Zones (OMZs). These OMZs occur in poorly ventilated areas, below productive surface regions (between 200 and 600 m) and are defined by O_2 thresholds representing different stress levels on the marine ecosystem. In this study, we followed Bopp's and Cocco's definition [2, 3] with thresholds defined as $80\,\text{mmol m}^{-3}$, $50\,\text{mmol m}^{-3}$ and $5\,\text{mmol m}^{-3}$, corresponding to distinctive effects

on biogeochemistry (respectively oxygen stress for marine organisms including Atlantic Ocean's species, hypoxia: a shortage of oxygen for life processes, and suboxia: O_2 conditions conducting to denitrification and anaerobic ammonium oxidation). OMZs have been shown to expand in the context of a global ocean deoxygenation attributed to global changes [4–8]. The upper ocean has lost 0.5%–3.3% of oxygen since the 1970s [9]. Moreover, the deoxygenation and OMZs expansion is expected to continue throughout the 21st century. This additional deoxygenation taking place over the next 100 years is estimated between 1%–7% of the current global inventory according to ocean climate model projections and different climatic scenarios [2, 10], but is potentially underestimated according to the recent Coupled Model Intercomparison Project (CMIP6) [11]. In addition, decreasing marine O_2 has been shown to intensify marine hypoxia, thereby compressing the habitat of aerobic organisms [12], influencing biogeochemical processes (e.g. the remineralization of OM and the nitrogen cycle, [13]) and ecosystem diversity, leading to potentially severe socioeconomic impacts [14].

Although the ultimate solution would be to drastically reduce anthropic greenhouse gases (GHG) and nutrient pollution, anthropogenic reoxygenation has been proposed as a potential mean to mitigate deoxygenation. Despite the uncertainties regarding the origin of hypoxia, engineering methods have been tested to mitigate their expansion (with modeling and in-situ approaches) in some lakes [15] and coastal marine environments, with contradictory results [16]. For example, similar conceptual oxygenation techniques (artificial downwelling of oxygen-rich water) were carried out in two different regions resulting in either an *in situ* deep water oxygen restoration in the By Fjord [17] or a modeled Pacific desoxygenation and changes in biological activity beyond the experimental sites [1].

An evaluation of the direct O_2 injection effects at global scale has, to our knowledge, never been carried out. Thanks to the electrolysis of water used to produce green hydrogen, which generates O_2 as a byproduct, the injection of O_2 is now conceivable at global scale into the ocean. Indeed, hydrogen produced by water electrolysis from renewable energy (e.g. from offshore wind farms) is now widely seen as green hydrogen given its low environmental footprint [18] and has therefore been recently subjected to high investment by developed countries and foreseen to be widely used among the global population.

The current study aims to assess the potential of this anthropogenic oxygen (AO) injection into the ocean and its environmental impact using a specifically designed global scenario with a coupled physical-biogeochemical model.

2. Experimental setup
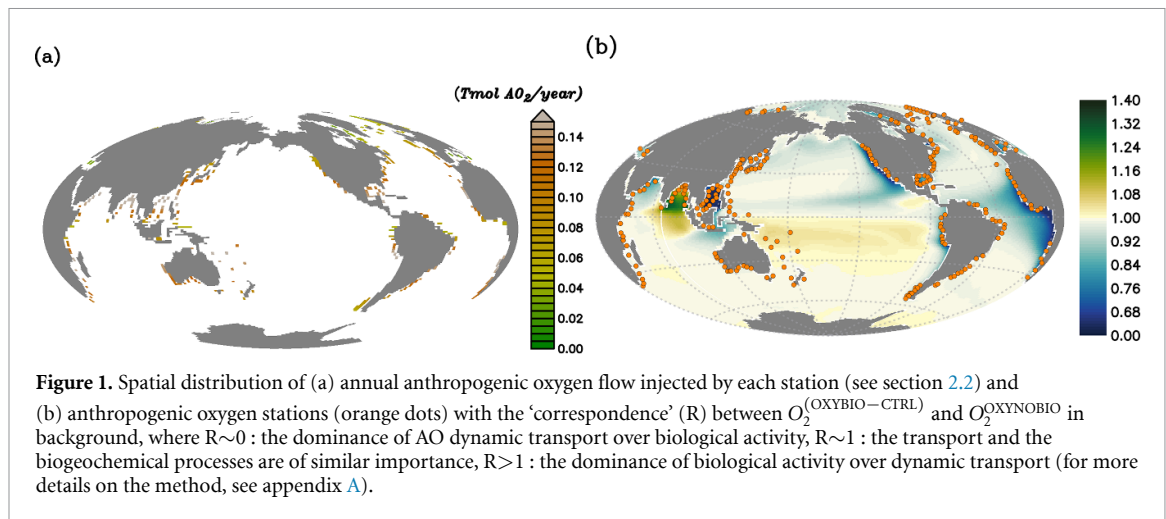
2.1. Numerical models used

We used the Nucleus for European Modelling of the Ocean (NEMO) platform (version 4.0). The NEMO platform comprises an ocean dynamical (NEMO-OCE in a ORCA2 configuration [19]), a sea ice (NEMO-ICE) and a biogeochemical model (NEMO-PISCES) to simulate the ocean at global scale. The biogeochemical component, named Pelagic Interaction Scheme for Carbon and Ecosystem Studies (PISCES-v2), is an intermediate complexity marine ecosystem model simulating the main biogeochemical cycles and the first trophic levels. Four main living compartments are simulated (two phytoplankton and two zooplankton functional groups) as well as detritus (including two size classes, small and large organic particulate carbon (POC)), nutrients and O_2 [20]. As an extensive description and validation of the model has been published in [20], therefore only the relevant parts of the model are recalled here.

In the model, air–sea O_2 exchange is computed using the commonly used Wanninkhof's parameterization [21]. O_2 concentration in the ocean depends mostly on photosynthesis (O_2 production) and remineralization (O_2 consumption) with a O_2/C Redfield ratio equal to 1.34 [22]. Denitrification process (i.e. the use of the oxygen from nitrate (NO_3) when O_2 concentration lower than 6 μM [23]) is explicitly simulated in PISCES.

The relative complexity of the O_2 cycle in the NEMO-PISCES model results in good abilities to (i) represent volumes of low oxygenated waters at global scale [2] (figure C1(b)), and (ii) simulate a reasonable mean state compared to other global biogeochemical models [24, 25] used in CMIP. These good performances explain our choice of using the NEMO-PISCES model for the present study.

2.2. Simulation setup

We used the PISCES model forced offline by an ocean dynamical seasonal climatology as in [20]. The model spatial horizontal resolution is 2° by 2° $\cos\phi$ (where ϕ is the latitude) with a meridional resolution refined to 0.5° near the equator. The vertical grid is composed of 31 layers of widths varying between 10 m near the surface to 500 m at depth. Prior to our experiments, we have spun up the biogeochemical model for 2000 years, starting from observed climatologies for nutrients [26] and from uniform low values for ecological tracers, until quasi-equilibrium was reached. After this spin-up, 100 additional years were simulated in two different configurations: (1) a control simulation (CTRL) without AO perturbation, (2) a simulation with an added AO (OXYBIO). A third configuration, named OXYNOBIO, simulates AO as a conservative passive tracer regardless of the oxygen cycle, with the exact same source of AO than

Figure 1. Spatial distribution of (a) annual anthropogenic oxygen flow injected by each station (see section 2.2) and (b) anthropogenic oxygen stations (orange dots) with the 'correspondence' (R) between $O_2^{(OXYBIO-CTRL)}$ and $O_2^{OXYNOBIO}$ in background, where R~0 : the dominance of AO dynamic transport over biological activity, R~1 : the transport and the biogeochemical processes are of similar importance, R>1 : the dominance of biological activity over dynamic transport (for more details on the method, see appendix A).

the one used in OXYBIO. The aim of simulating the OXYNOBIO tracer is to track the transport of AO over a span of 100 years.

The experimental scenario used for the AO injection was based on the theoretical economical viability and industrial feasibility of offshore implantation of hydrogen Production Units (PUs). Offshore locations have been gauged considering socioeconomic and technological data mainly in line with the forecasts from the International Energy Agency [27]. These theoretical locations were provided by the LHYFE company [28] which is a producer and supplier of green hydrogen. This idealized scenario was designed to give an upper bound of an AO injection by assuming a global adoption of hydrogen as a key component of renewable energy supply chains by 2030, which corresponds to the highest level of plausible green hydrogen use.

For this study, the assumed number of hydrogen plants installed over the next 50 years follow roughly the same deployment than the offshore oil platforms between 1975 and 2020: approximately 20 000 platforms. A scenario allowing the deployment of 17 936 PUs has therefore been defined. The PUs have been distributed within 304 selected model grid points (each covering about 400 000 km^2, called hereafter 'stations'), resulting in an average of 59 PUs per model grid point. These stations were distributed along the world's coasts (figure 1) according to the combination of two criteria: (i) an average wind speed preferably between 12–17 m s^{-1} (optimal operation of the wind turbines) or between the minimum and maximum wind speed needed to operate the wind turbine (5–25 m s^{-1} [27, 29]), and (ii) a population density that is presumed to exceed 2000 people km^{-2} (related to the size of the energy market), or display a constant or even positive natural evolution of the population by 2050 [27, 30]. As a result, the locations of the PUs are not necessarily positioned near known OMZs. Finally, we chose an injection depth of 150 m, except in areas with shallower bathymetry where the AO was injected at the greatest depth

possible. Indeed, injection at a depth exceeding 150 m (e.g. close to the core of the OMZ) would have been more costly and would therefore not be economically viable. Nevertheless, the depth chosen here remains close to the upper limit of the OMZ [31] (figure C1).

Currently, the green hydrogen production can reach or even exceed 129 000 t H$_2$ y^{-1}, depending on the PU [28]. During the production of hydrogen by electrolysis, the H$_2$/O$_2$ ratio is 2:1 [32]. This amounts to 8 kg of O$_2$ per 1 kg of H$_2$ produced. Thus, according to LHYFE's forecasts, each of the PUs would produce 70 000 t O$_2$ y^{-1} (figure 1(a)), i.e. 39.2 Tmol y^{-1} globally, which corresponds to ⌣0.86% of the overall biogenic O$_2$ production in the CTRL simulation between 0–150 m (4.56 Pmol y^{-1}).

It is important to note that the idealized setup of our experimental design leaves aside engineering injection details (discussed in section 3.5) that may impact the efficiency of the AO injection.

3. Results and discussion

3.1. (De)oxygenation and OMZs widespread changes induced by anthropogenic oxygen injection

After 100 years of AO injection (OXYBIO run), the global O$_2$ inventory increased by 0.07% with respect to the CTRL run (estimated to be 233.1 Pmol, a value close to that obtained from the observations by [8]: 227.4 Pmol). Yet, the AO injection reduced the volume of OMZs by between 1.1% and 2.4%, depending on the O$_2$ concentration threshold used (table 1). This suggests that the overall evolution of the OMZ volume is weakly sensitive to the chosen threshold. However, the global average hides significant regional disparities.

The OMZs that shrank the most are the least extended (figure 2(a), table 1): in the Atlantic Ocean and the Arabian Sea (AS), that shrank by 13.3%–35.6% and 3.4%–6.1% respectively (80 mmol m^{-3} and 50 mmol m^{-3} thresholds). The

Table 1. The proportion of the volume of each OMZ to the overall volume of OMZs (volume contribution) at the last simulated year of the CTRL run and averaged between 200 and 600 m depth, and change (OXYBIO minus CTRL) in volume of the oxygen-poor water (generically referred to as OMZs) after 100 years of AO injection. The volumes are defined by oxygen thresholds 80 mmol m^{-3}, 50 mmol m^{-3} and 5 mmol m^{-3}. Free fields (*) represent the absence of water masses with O_2 concentrations below 5 mmol m^{-3} and bold indicates values for OMZs at global scale (sum of OMZs).

OMZ	80 mmol m^{-3}		50 mmol m^{-3}		5 mmol m^{-3}	
%	Change	Volume contribution	Change	Volume contribution	Change	Volume contribution
Global	**−2,4**	**100**	**−1,1**	**100**	**−1,1**	**100**
Atlantic Ocean	−13,3	6,6	−34,6	4	0	2,4
Pacific Ocean	−2,3	81,3	−0,6	86,1	−2	94,6
Bay of Bengal	+5,5	8,1	+11,6	7,9	+25,3	3
Arabian Sea	−3,4	4,1	−6,1	2	*	*

Figure 2. (a) Spatial distribution of the annual mean O_2 concentration of the last simulated year of the CTRL run (mmol m^{-3}) averaged between 200 and 600 m depth, the typical depth range of the main OMZs. The area of concentration below 80 mmol m^{-3} is outlined in grey. (b)–(f) Changes in annual mean O_2 concentration (OXYBIO minus CTRL) after 100 years of AO injection (b) averaged between 200 and 600 m depth (mmol m^{-3}), and (c)–(f) along meridional sections (%), in (c) the Atlantic Ocean at 2 °E, (d) the Pacific Ocean at 120 °W, (e) the Bay of Bengal at 90 °E and (f) the Arabian Sea at 70 °E. In (c)–(f), the isopleths at 50 and 80 mmol m^{-3} are shown in blue for the CTRL simulation and in orange for the OXYBIO simulation, and the black solid lines show the isopycnals that delimit the water masses based on water masses definition in the appendix B.

smallest shrinkage (0.6%–2.3%) is that of the Pacific Ocean OMZ (table 1). The most striking consequence of the AO injection is simulated in the Bay of Bengal (BoB) where the OMZ expands counterintuitively, its volume increases by 5.5%–11.6% for the 80 mmol m^{-3} and 50 mmol m^{-3} thresholds, and even 25.3% for the 5 mmol m^{-3} threshold (table 1 and figure 2(b)).

Contrary to the global assessment, the volume variation of regional OMZs depends strongly on the threshold that is considered to define them. The harshest thresholds specific to each region allow us to determine the evolution of the OMZ core. Thus, excluding the Pacific OMZ, the volume change is the most relevant in the OMZ core (i.e. a larger volume variation for the threshold of 50 mmol m^{-3} in the Atlantic Ocean and 5 mmol m^{-3} in the AS and BoB than for 80 mmol m^{-3}, table 1). However, the evaluation of the structure of an OMZ requires to also consider its upper and lower boundaries (oxyclines)

[31]. OXYBIO configuration simulated a slight deepening of the upper oxycline of all OMZs (figures 2(c)–(f)), more marked in the Atlantic Ocean. Thus, their thickness thins by an average of 42 m (for the Atlantic Ocean) and 13 m (for the AS) between 0 and 600 m while that of the BoB thickens by 11 m despite the substantial increase in O_2 between 100 and 200 m, which can exceed 100% (figure 2(e)). The shift of the horizontal boundaries position of the OMZs in addition to the deepening of the vertical boundaries, characterize the strongest shrinkage of the OMZs, namely in the Atlantic Ocean, and to a lesser extent in the AS (figures 2(c) and (f)).

3.2. Mechanisms involved in the evolution of OMZs

A wide range of ecosystem processes interacting with the three-dimensional circulation determine the distribution of O_2 concentrations in the ocean [33]. The analyses in section 3.1 suggest a regional disparity in the mechanisms causing O_2 variation. O_2^{OXYNOBIO} (AO in the OXYNOBIO configuration) tracks exclusively the transport of AO without any air–sea exchanges and biogeochemical reactions. The correspondence (R) between the variation of O_2^{OXYNOBIO} and that of $O_2^{(\text{OXYBIO}-\text{CTRL})}$ (i.e. O_2 change) addresses the relative importance of biological activity and transport to O_2 variation in OXYBIO (figure 1 (b), equation (1) and appendix A).

$$R = \frac{\text{Variance} \left(O_2^{(\text{OXYBIO}-\text{CTRL})} - O_2^{\text{OXYNOBIO}} \right)}{\text{Variance} \left(O_2^{\text{OXYNOBIO}} \right)}. \quad (1)$$

R contrasts O_2 changes due to biological response (i.e. $O_2^{(\text{OXYBIO}-\text{CTRL})}$ minus O_2^{OXYNOBIO}) to AO transport (O_2^{OXYNOBIO}). Thus, in (figure 1(b)) the mechanisms are categorized as follow:

(i) R$\backsim$0 indicates the dominance of AO dynamic transport over biological activity as a mechanism for the variation of O_2,

(ii) R$\backsim$1 indicates that transport and biogeochemical processes are of similar importance to the O_2 changes. This suggests either a biological change concomitant with AO transport or transport of what result from remote biological response,

(iii) R>1 indicates the dominance of biological activity over dynamic transport to explain the variation of O_2 consecutive to AO injection.

Along the coastlines with injection sites, in the Atlantic Ocean and across the North Pacific Equatorial Current, the correspondence is high (R$\backsim$0). In the Atlantic Ocean, the OMZ shrank even where it is devoid of AO stations (figure 1(b)). Advective transport is therefore the driving factor feeding AO into this OMZ. Since this OMZ is included in the North Atlantic Central Water
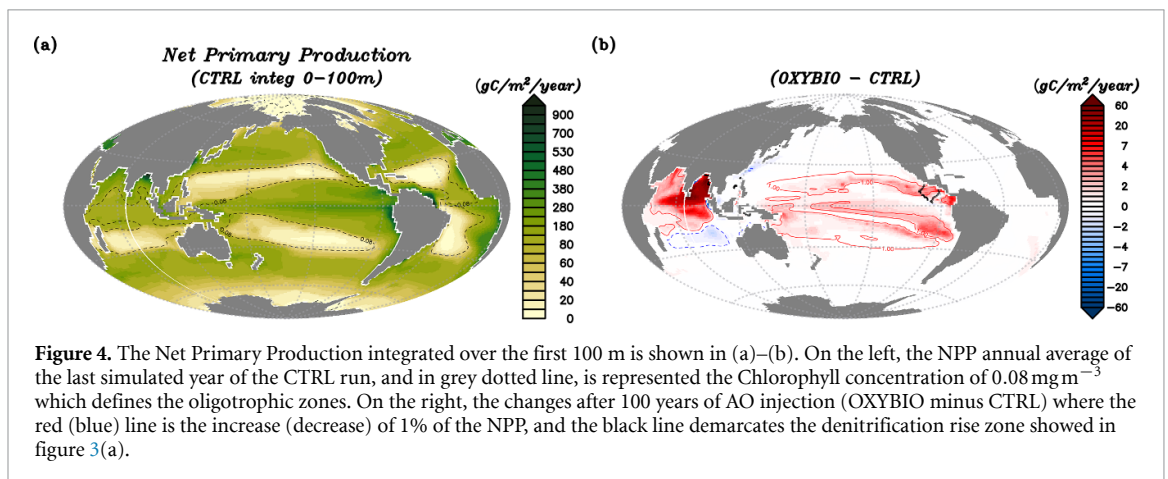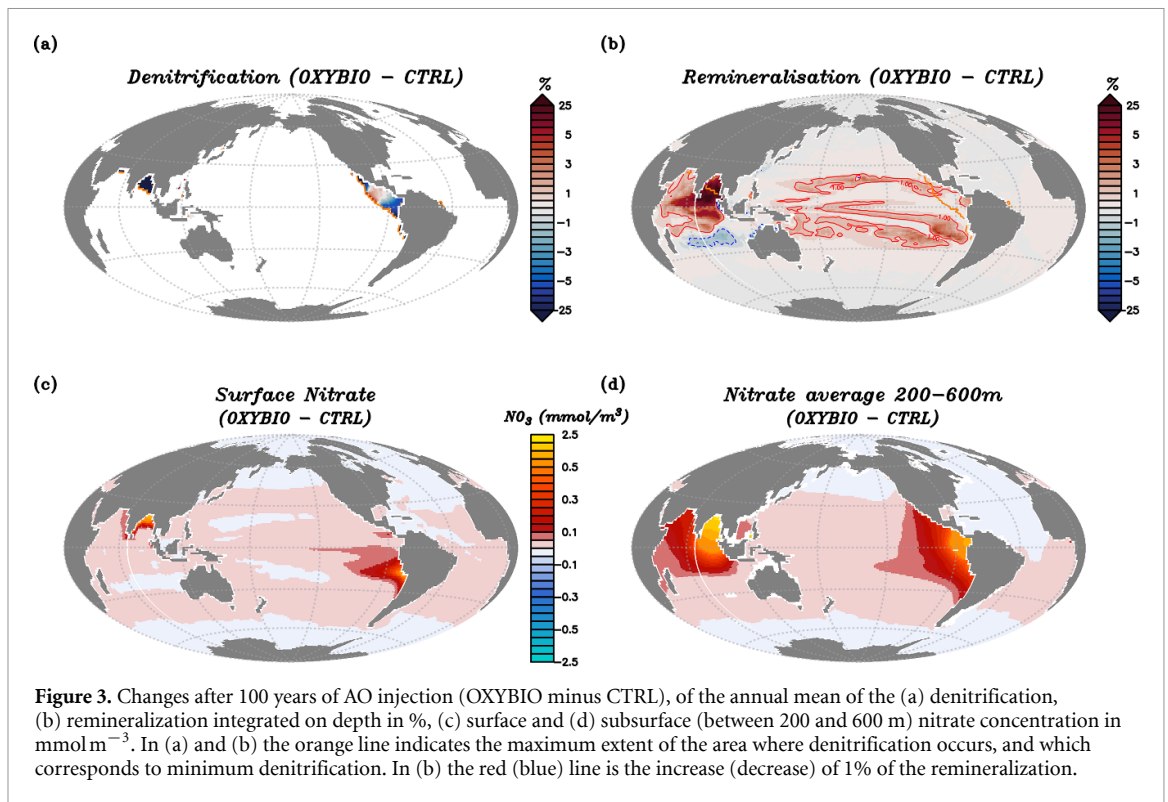
(figure C2) and has its top located in the Subtropical Mode Water (figure 2(c)), it could benefit from an efficient supply of AO. This OMZ would therefore be fed by the small cell-dominated by meridional surface transport as well as by the upper limb of the Atlantic Meridional Overturning Circulation (AMOC, figure C2). An exact quantification of this would require a dedicated study. In the South Pacific Ocean and the Costa Rica Dome, a combined effect of biogeochemical feedbacks and dynamic transport (R$\backsim$1) seems to explain the response to AO injection (figure 1(b)).

In the Indian Ocean, biogeochemical feedbacks dominate, especially in the BoB (R>1, figure 1(b)) where they appear to explain the counter-intuitive reduction of O_2 concentration in the OXYBIO simulation with respect to CTRL (figure 2(b)) as treated in section 3.3. It is noteworthy that the different biogeochemical responses between the AS and BoB is likely due to different levels of oxygen deficiency [34].

3.3. Impacts on nutrient recycling and biological activities

In the ocean, O_2 is consumed by biological respiration, including OM remineralization. When the waters become suboxic, oxygen from NO_3 is used for remineralization, a process called denitrification. OM remineralization is thus an internal source of 'recycled' fixed nitrogen (N) except in suboxic waters where denitrification is a sink of bioavailable nitrogen. In this section we investigate the potential cascading effects of the AO on the denitrification, remineralization, and Net Primary Production (NPP) (figures 3 and 4).

Denitrification is absent in the Atlantic Ocean OMZ (figure C3) due to relatively greater natural ventilation than in the other OMZs. The decrease (up to 10% in the Pacific Ocean) or even total inhibition (in the BoB) of denitrification in response to AO injection (figure 3(a)) reduces the NO_3 sink in initially (before AO injection) suboxic areas (figure 3, orange line). Note that at the surface, nutrients decrease except NO_3 which increases (figure 3(c)), while at the subsurface all nutrients increase (figures C4, C5 and 3(d)). This suggests that the reduction of denitrification is likely to increase the availability of NO_3 inducing the stimulation of NPP (figure 4(b)), thus increasing the exported production (figure 5(a)). As remineralization is constrained by OM [35–37], the additional supply of OM can thus amplify and maintain high remineralization leading to an increase in deep nutrient stocks [1]. Indeed, the seasonal thermocline of BoB is a major nutrient reservoir through the intense remineralization of exported OM [38]. However, by increasing NPP, nutrient uptake is amplified. Thus, the originally non-limiting nutrients may decrease until depletion [39] as in the
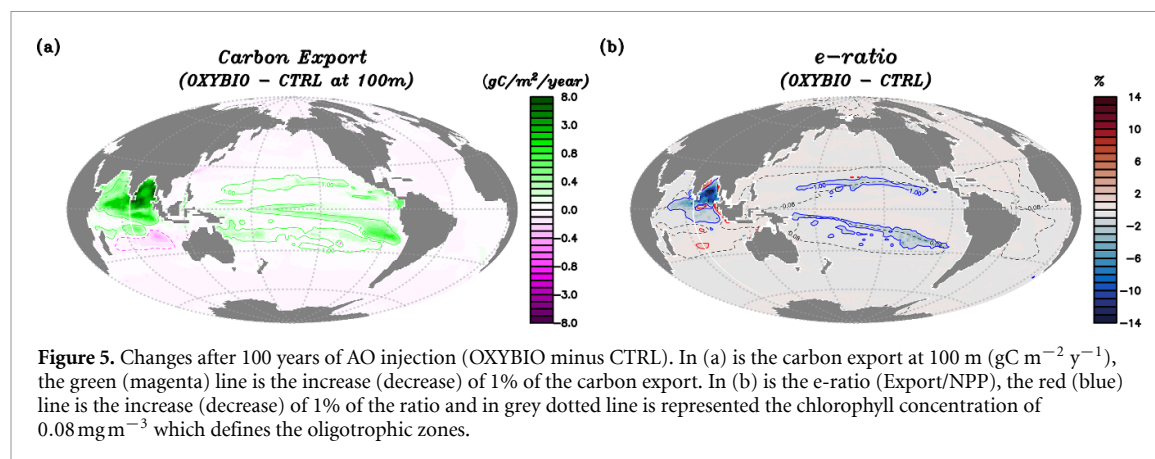
Figure 3. Changes after 100 years of AO injection (OXYBIO minus CTRL), of the annual mean of the (a) denitrification, (b) remineralization integrated on depth in %, (c) surface and (d) subsurface (between 200 and 600 m) nitrate concentration in $mmol\,m^{-3}$. In (a) and (b) the orange line indicates the maximum extent of the area where denitrification occurs, and which corresponds to minimum denitrification. In (b) the red (blue) line is the increase (decrease) of 1% of the remineralization.

Figure 4. The Net Primary Production integrated over the first 100 m is shown in (a)–(b). On the left, the NPP annual average of the last simulated year of the CTRL run, and in grey dotted line, is represented the Chlorophyll concentration of $0.08\,mg\,m^{-3}$ which defines the oligotrophic zones. On the right, the changes after 100 years of AO injection (OXYBIO minus CTRL) where the red (blue) line is the increase (decrease) of 1% of the NPP, and the black line demarcates the denitrification rise zone showed in figure 3(a).

BoB where NO_3 limitation shifts to phosphate limitation for nanophytoplankton and changes from silicate to phosphate limitation for diatoms (figure C6).

In conclusion, the expansion of OMZ indicates an imbalance between oxygen supply and biological O_2 consumption, as in the case of BoB. Despite continuous oxygenated water injection and O_2 transport through ocean dynamics, biological activity can still drive an expansion of an OMZ in some regions. The suppression of the nitrate sink (by inhibiting denitrification) and enhancing nutrient recycling (through remineralization) particularly at the seasonal thermocline is the cause. Moreover, the decline of the denitrification results in a decrease in nitrogen fixation (N_2-fixation, roughly 50% in the vicinity of BoB) (figure C7). Landolfi's study [40] emphasized the vicious cycle induced by the spatial coupling of

denitrification and N_2-fixation. Due to stoichiometric imbalance, The NO_3 loss through denitrification versus the nitrogen gain through the OM remineralization derived from N_2-fixation leads to a net loss of fixed nitrogen that further stimulates N_2-fixation. Counter-intuitively, the reduction in N_2-fixation in the OXYBIO simulation, through the ihnibition of denitrification, could thus contribute to an increase in fixed nitrogen.

The other consequence particularly notable is the nonlocal environmental effects of AO injection. The AO stimulates biological activities beyond the zones of O_2 change, especially in the Indian and tropical Pacific Oceans, except in the Northern Hemisphere where O_2 changes and biological activities tally (figure 1(b)). While denitrification changes are mainly confined to the continental margins

Figure 5. Changes after 100 years of AO injection (OXYBIO minus CTRL). In (a) is the carbon export at 100 m (gC m^{-2} y^{-1}), the green (magenta) line is the increase (decrease) of 1% of the carbon export. In (b) is the e-ratio (Export/NPP), the red (blue) line is the increase (decrease) of 1% of the ratio and in grey dotted line is represented the chlorophyll concentration of 0.08 mg m^{-3} which defines the oligotrophic zones.

(figure 3(a)), remineralization changes are remotely triggered (figure 3(b)). Whether it is related to aerobic respiration (figure 3(b)) or NPP (figure 4(b)), biogeochemical changes follow the pathways of the advective currents (i.e. circulation of the subtropical gyres) (figures 1(b) and 4). In the Eastern Pacific Equatorial zone, phytoplankton is mainly Fe-limited in the CTRL simulation (figure C6). Thus, the gain in NO$_3$ (figures 3(c) and (d)), due to reduced denitrification in this zone, would feed the initially NO$_3$-limited phytoplankton communities in the areas surrounding the Pacific cold tongue and along the Central American coasts (figures C6(a) and (c)), through lateral surface transport. As a result, NPP increases north of the equator (figure 4(b)) along the Central American coasts (from the Gulf of Panama to the Mexican coast), where there are no injection stations (figure 1). This local NPP increase would trigger O$_2$-consuming remineralization (figure 3(b)). Thus, the Costa Rica Dome, an eddy structure particularly influenced by the Costa Rica Coastal Current from the south, would be subject to exacerbated denitrification (up to 5%, figure 3(a)) due to this stimulation of remineralization bordering the dome. In the Tropical South Pacific Ocean, the edges of the denitrification zones (where it is lowest (figure C3), indicated by the orange line in figure 3(a)), show the largest decrease in denitrification, by 4%. Beyond these edges, the NPP remote response (rising to +3% off Chile (figure 4(b)) is triggered by the new supply of NO$_3$ in zones that can be limited in NO$_3$ (figure C6), which could explain the lack of NPP response near coasts where phytoplankton is mainly limited by Fe and Si (figure C6). Hence, these biogeochemical changes would be transported along the South Equatorial Current, feeding the subtropical gyre through the lateral transport [41].

Another striking region is the Indian Subtropical oligotrophic gyre (figure 4(a)), where the biological response is opposite to all other basins (figures 3(b) and 4). In BoB, the strong increase in NPP results in increased nutrient consumption (figure C4). This drop in nutrients could lead to a reduction in

the supply of nutrients to the Indian Subtropical gyre through the South Java Current and explain the NPP decrease. In such a 'regenerative loop' regime [42] where most production is driven by recycled nutrients [43], the small reduction in OM remineralization may also explain the decrease in NPP in a chain-reaction.

3.4. Overview of the carbon cycle implications

Fertilization, whether natural [44] or artificial [45], can favor exported production through the development of ecosystems prone to exceptional blooms. These ecosystems are based on a biomass dominated by large cells (e.g. diatom [46–48]) and a NPP provided jointly by small and large cells [49]. The AO injection-induced denitrification inhibition does not appear to lead a change in the phytoplankton community despite NO$_3$ enrichment (figure C8). Besides phytoplankton community composition, estimation of NPP is important for inferring the additional sequestered carbon. AO injection-induced NPP increase (+0.7%) is close to the magnitude of the decrease predicted by the low-emission scenario SSP1-2.6 ($-0.56 \pm 4.12\%$) but is less than the decrease predicted by the high emission scenario SSP5-8.5 ($-2.99 \pm 9.11\%$) by 2100 [11], which assumes a potentially negligible effect on the overall air–sea CO$_2$ flux.

Because of the ability of artificial oxygenation to increase nitrogen concentration, it can also be suggested as an indirect means of fertilization by industry to stimulate the carbon pump. Yet, iron fertilization experiments revealed inconsistent export of production despite increased NPP [50]. In our study, despite the joint increase in NPP and exported production (figures 4(b) and 5(a)), the e-ratio decreases between 1%–14% depending on the region (figure 5(b)), which indicates a decrease in the efficiency of carbon export. Thus, due to a regionally variable duality between remineralization processes and OM export beyond injection sites, the effect of AO on carbon storage should not be overlooked in future studies.

3.5. Uncertainties regarding the AO injection impacts and the representation of biogeochemical processes

Several sources of uncertainty are possible when analyzing the effects of AO injection on the global ocean. The deployment scenario used in this study may represent one of them and may affect the results. For example, the choice of injection depth is constrained by structural robustness and cost. However, at 1000 m the oxygen utilization rate is 10 to 50 times lower than at 100 m [10, 51–54]. Hence, depth is an important causal parameter in the biogeochemical and ecosystem response to AO injection. The coarse resolution of the model used ($2°$ resolution) prevents us from documenting technologies required to inject AO, which come under sub-grid processes but may affect AO efficiency [1, 15]. Yet, we can infer that AO should be undersaturated at the injection sites (figure C9). Thus, O_2 saturation at injection sites (with no technical limitation taken into account) would allow the full dissolution of the AO. In addition, the spatial resolution implies process-related biases below the mesoscale spectrum [55]. Regional modeling of the AS highlighted the importance of eddy-induced advection on vertical and lateral O_2 transport [56]. Increasing the resolution improves the explicit representation of eddy mixing that would be involved in the biased volume representation of OMZs in noneddy resolving ocean models. Thus, eddy mixing may be crucial in shaping marine habitats of oxygen-sensitive species [57].

Numerical modeling of OMZs and their ecosystems is an important socioeconomic issue because they are important fishing areas [58–60]. However, the current ocean microbiome modeling remains simple compared to the complexity that emerges from observations [61]. Also, AO injection showed that the evolution of carbon transfer to the deep ocean [62] as well as the fate of the OMZs, and consequently of the fisheries [58–60], require the analysis of phytoplankton and zooplankton communities. In our study, the microbial recycling mechanisms are parameterized lacking an explicit representation of bacterial communities despite the influence of O_2 on controlling the availability of fixed nitrogen in the ocean [63, 64]. Regionally, explicit modeling of some ecosystems can improve the simulation of these processes, such as the diazotrophic community in the Tropical Pacific [65], especially since the anaerobic to aerobic transition in the ocean can cause strong negative feedback on nitrogen fixation [64]. Ultimately, ecosystem diversity differs according to the model used, and uncertainties in their applications remain [3, 61, 66, 67] and limit management or geoengineering decisions that are based solely on the use of models [68].

Despite these uncertainties, our results describe changes in biogeochemical processes in line with published regional studies on the effects of changing oxygen levels (e.g. in the Arabian Sea [57]). In the Pacific ocean, oxygenation through the modification of modeled vertical water exchange have also ultimately resulted in a deoxygenation and remote changes in biological activity [1]. However, given that biogeochemical processes tend towards a new equilibrium state after 20 to 40 years of simulation, as in BoB (not shown), we do not prejudge the effects of extending the experiment, nor of stopping the injection, either during or after the 100 year experiment, which could potentially lead to a global and regional new state.

4. Concluding remarks

Although model limitations must be kept in mind, our AO injection scenario reveals weak global oxygenation ($+0.07\%$). Comparatively, CMIP models predict deoxygenation between 2.2% (SSP1-2.6 scenario), i.e. 30 times the oxygenation induced by AO, and 4.5% (SSP5-8.5 scenario) [11]. However, OMZs shrinkage (table 1) is in the lower limit of the OMZs expansion predicted by the RCP-8.5 scenario (between 1%–16% depending on the different CMIP5 models and thresholds [2]). Regionally, our study reveals deoxygenation and subsequent BoB OMZ expansion related to the dominance of biogeochemical processes, as well as non-local environmental effects in the Pacific and Indian Oceans, where biogeochemical and dynamic processes may be of similar importance. They are the result of the disruption of the nitrogen cycle through the inhibition of denitrification. The response of the Atlantic OMZ, devoid of denitrification, is marked by the AO transport allowing its shrinkage.

Given the uncertainties that may arise from both the scenario and the tools used, as discussed in section 3.5, regional and high-resolution studies are therefore needed to better understand the effects and risks of AO on benthic and pelagic ecosystems, higher trophic levels, and microbial communities, even on fisheries.

Data availability statement

The data that support the findings of this study are openly available at the following URL/DOI: https://doi.org/10.5281/zenodo.7377078. The data [69] are restricted by an access request.

Atlantic climate-based marine ecosystem prediction for sustainable management; H2020 Grant Agreement No. 817578).

Appendix A. Calculation of the correspondence

By analogy with the method used by Vinogradova *et al* 2007 and Bingham and Hughes 2008, we employed correspondence analysis to determine the extent to which anthropogenic O_2 transport is involved in the variability of O_2 over the 100 year injection period. Let O_2^{OXYNOBIO} be the evolution of the AO concentration during the 100 years of injection (O_2 as a passive tracer), and O_2^{OXYBIO} the evolution of the O_2 concentration during the 100 years of injection (i.e. oxygen varying with transport, biological activity, air-sea exchange, and in response to the AO injection). The correspondence is an adimentional value based on the estimation of the ratio between the variance of the difference between $O_2^{\text{OXYBIO}-\text{CTRL}}$ and O_2^{OXYNOBIO} and the variance of O_2^{OXYNOBIO} alone. Thus, we can compare whether:

(i) $R \curvearrowright 0$ indicates minor variation in biological activity ($O_2^{(\text{OXYBIO}-\text{CTRL})}$ - O_2^{OXYNOBIO}) compared to dynamic transport (O_2^{OXYNOBIO}), as well as concomitant variation in $O_2^{(\text{OXYBIO}-\text{CTRL})}$ and O_2^{OXYNOBIO}, revealing the preponderance of dynamic transport of AO over biological activity as a mechanism for the variation of O_2;

(ii) $R \curvearrowright 1$ indicates that the factors that differentiate O_2^{OXYNOBIO} from $O_2^{(\text{OXYBIO}-\text{CTRL})}$ vary similarly to O_2^{OXYNOBIO}, so that biological activity varies similarly to the passive tracer transport. Thus, changes in O_2^{OXYBIO} are related to the transport of the biological activity outcome (such as organic matter (OM) and nutrients)

(iii) $R > 1$ corresponds to a strong discrepancy between $O_2^{(\text{OXYBIO}-\text{CTRL})}$ and O_2^{OXYNOBIO}, and the variation of biological activities is greater than that of dynamic transport. Consequently, the mechanisms that cause O_2^{OXYBIO} change are more related to biological activity than to dynamic transport, whether it is that of AO or that of biochemical elements. These various responses imply contrasted evolution of OMZs.
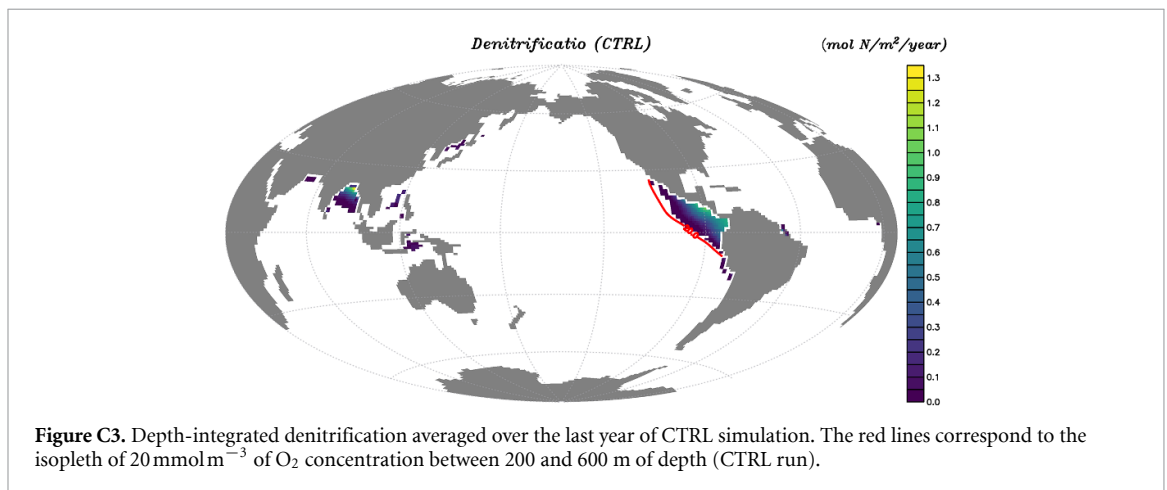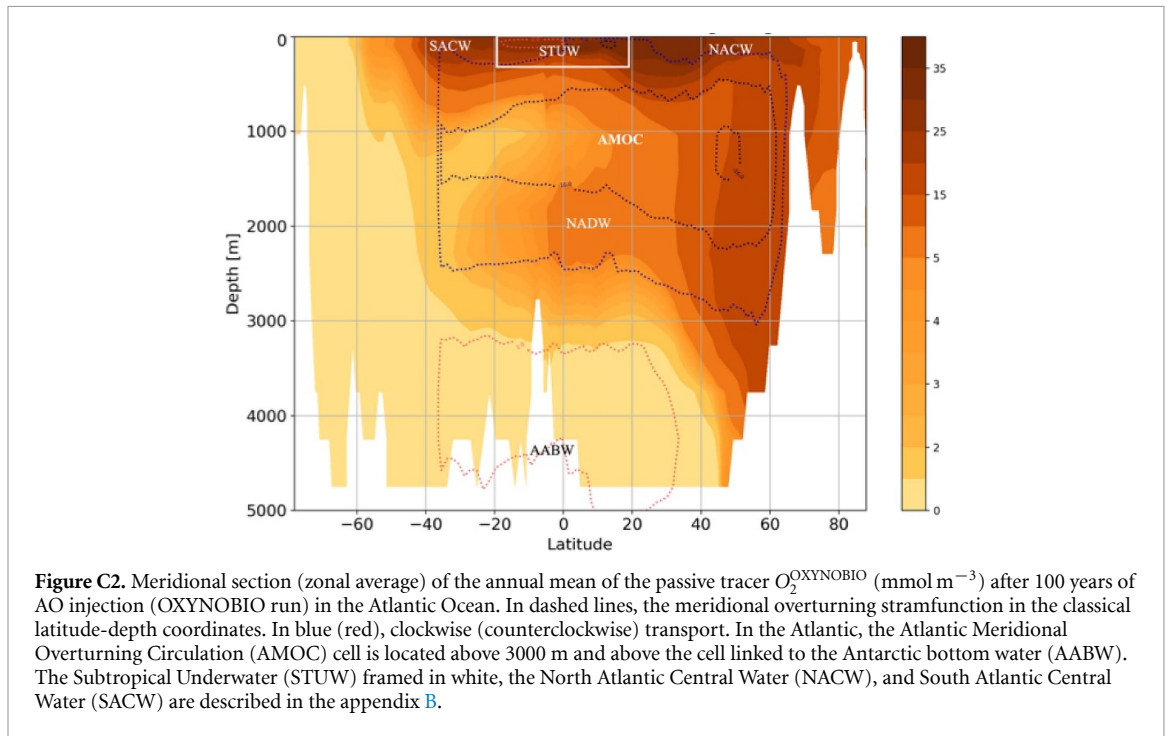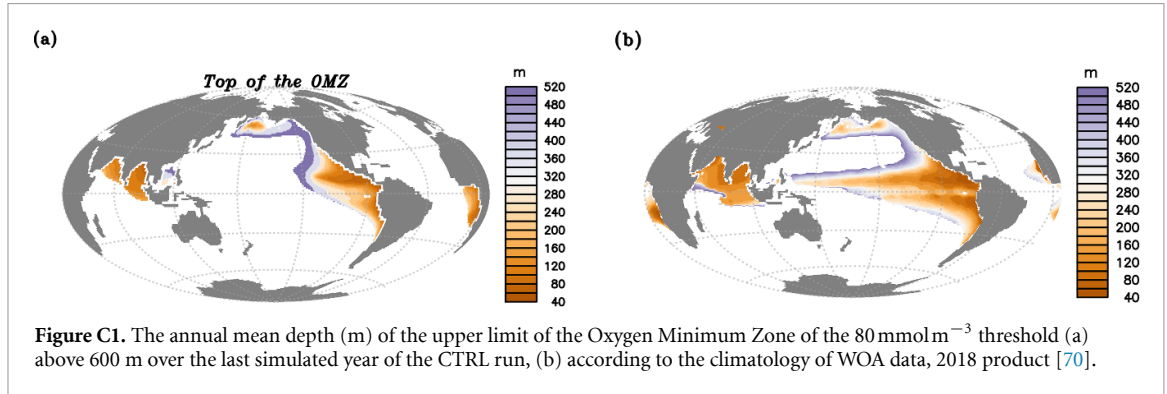
Appendix B. Definitions of water masses

The black solid lines in figures 2(c)–(f) show the isopycnes that delimit the water masses based on Talley *et al* 2011 and Pollard and Pu, 1985 (figure C2). In figure 2(c) Atlantic section at 2°E, the potential density $\sigma_0 = 25\,\text{kg}\,\text{m}^{-3}$ is the lower boundary to define the Subtropical Underwater (STUW), the North Atlantic Central Water is bounded between $\sigma_0 = 26.5\,\text{kg}\,\text{m}^{-3}$ and $27.3\,\text{kg}\,\text{m}^{-3}$ and including South Atlantic Central Water, between $\sigma_0 = 27.3$–$27.7\,\text{kg}\,\text{m}^{-3}$ is the Intermediate Water. In (d) Pacific section at 120°W, between $\sigma_0 = 24.5$–$26.5\,\text{kg}\,\text{m}^{-3}$ it is the 'thermocline' which includes subtropical mode waters and between $\sigma_0 = 26.5$–$27.65\,\text{kg}\,\text{m}^{-3}$ the 'intermediate waters' which includes subantarctic mode waters and North Pacific Intermediate Waters, and below is the 'deep ocean'. In (e) Bay of Bengal at 90 °E and (f) Arabian Sea at 70 °E, above $\sigma_0 = 26\,\text{kg}\,\text{m}^{-3}$ it is the STUW, the Subtropical Mode Water is between $\sigma_0 = 26$–$26.8\,\text{kg}\,\text{m}^{-3}$, below $\sigma_0 = 26.8\,\text{kg}\,\text{m}^{-3}$ these are the 'intermediate waters' these are the intermediate waters which include, in the Arabian Sea, the Red Sea waters.

B.1. References of appendices A and B

Vinogradova NT, Ponte RM, Stammer D. 2007 Relation between sea level and bottom pressure and the vertical dependence of oceanic variability. Geophys Res Lett. 34. https://doi.org/10.1029/2006GL028588. Bingham RJ, Hughes CW. 2008 The relationship between sea-level and bottom pressure variability in an eddy permitting ocean model. Geophys Res Lett. 35. https://doi.org/10.1029/2007GL032662. Talley LD, Pickard GL, Emery WJ, Swift JH. 2011 Descriptive Physical Oceanography. Ed Elsevier. https://doi.org/10.1016/C2009-0-24322-4. Pollard, R. T., & Pu, S. 1985. Structure and circulation of the Upper Atlantic Ocean northeast of the Azores. Progress in Oceanography, 14(C), 443–462. https://doi.org/10.1016/0079-6611(85)90022-9.

Appendix C. Additional figures

Figure C1. The annual mean depth (m) of the upper limit of the Oxygen Minimum Zone of the $80\,\mathrm{mmol\,m^{-3}}$ threshold (a) above 600 m over the last simulated year of the CTRL run, (b) according to the climatology of WOA data, 2018 product [70].

Figure C2. Meridional section (zonal average) of the annual mean of the passive tracer O_2^{OXYNOBIO} ($\mathrm{mmol\,m^{-3}}$) after 100 years of AO injection (OXYNOBIO run) in the Atlantic Ocean. In dashed lines, the meridional overturning stramfunction in the classical latitude-depth coordinates. In blue (red), clockwise (counterclockwise) transport. In the Atlantic, the Atlantic Meridional Overturning Circulation (AMOC) cell is located above 3000 m and above the cell linked to the Antarctic bottom water (AABW). The Subtropical Underwater (STUW) framed in white, the North Atlantic Central Water (NACW), and South Atlantic Central Water (SACW) are described in the appendix B.

Figure C3. Depth-integrated denitrification averaged over the last year of CTRL simulation. The red lines correspond to the isopleth of $20\,\mathrm{mmol\,m^{-3}}$ of O_2 concentration between 200 and 600 m of depth (CTRL run).
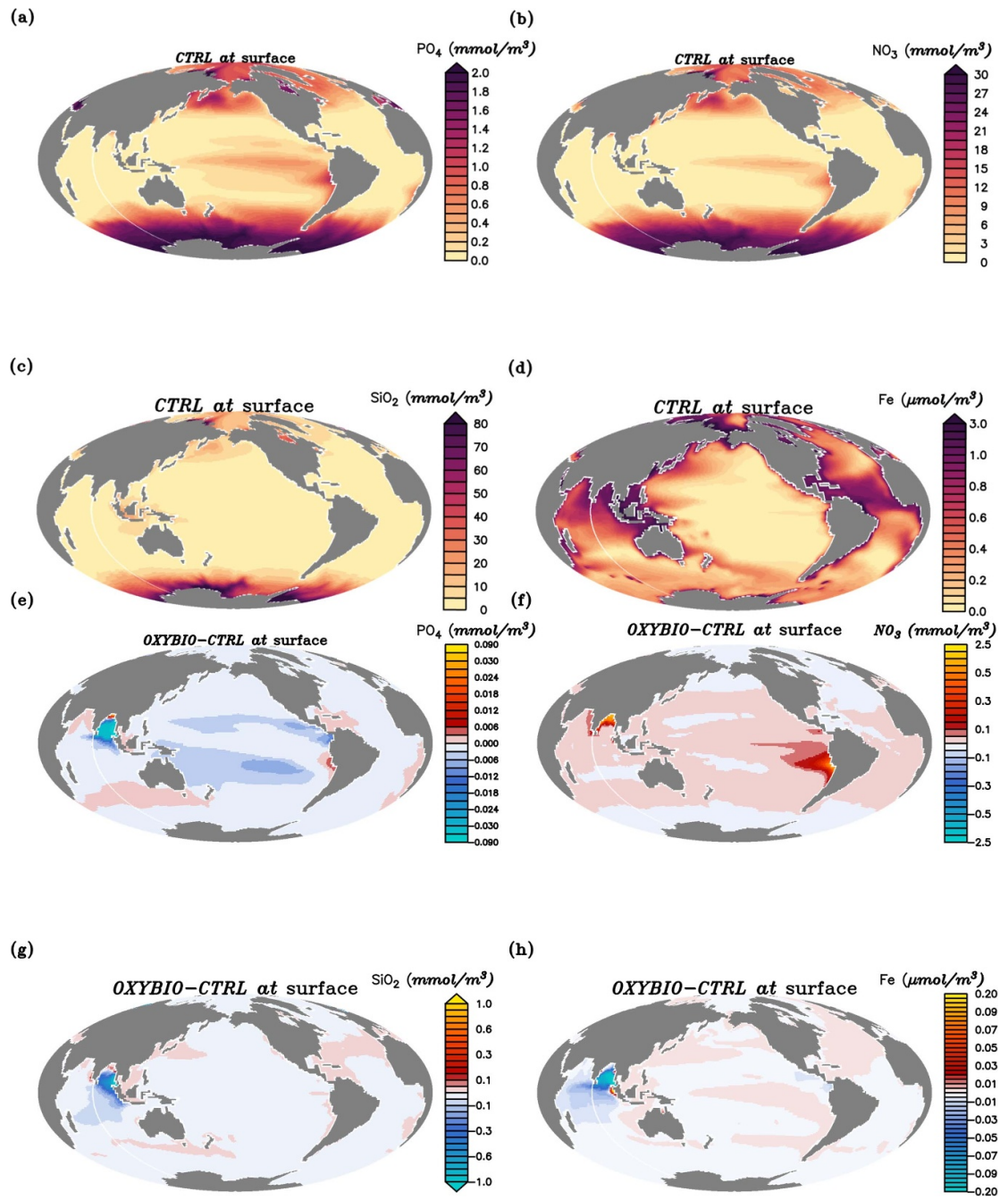
Figure C4. Annual mean surface concentrations of phosphate (PO_4), nitrate (NO_3), silicate (SiO_2), iron (Fe) over the last simulated year of the CTRL run (in mmol m^{-3} and ¦µmol m^{-3} for Fe) (a)–(d). Changes after 100 years of AO injection (OXYBIO-CTRL), of the annual mean surface concentrations of these nutrients (e)–(h).

Figure C5. Annual mean subsurface concentrations of phosphate (PO_4), nitrate (NO_3), silicate (SiO_2), iron (Fe) over the last simulated year of the CTRL run (in $mmol\,m^{-3}$ and $\mu mol\,m^{-3}$ for Fe) (a)–(d). Changes after 100 years of AO injection (OXYBIO-CTRL), of the annual mean subsurface concentrations of these nutrients (e)–(h).
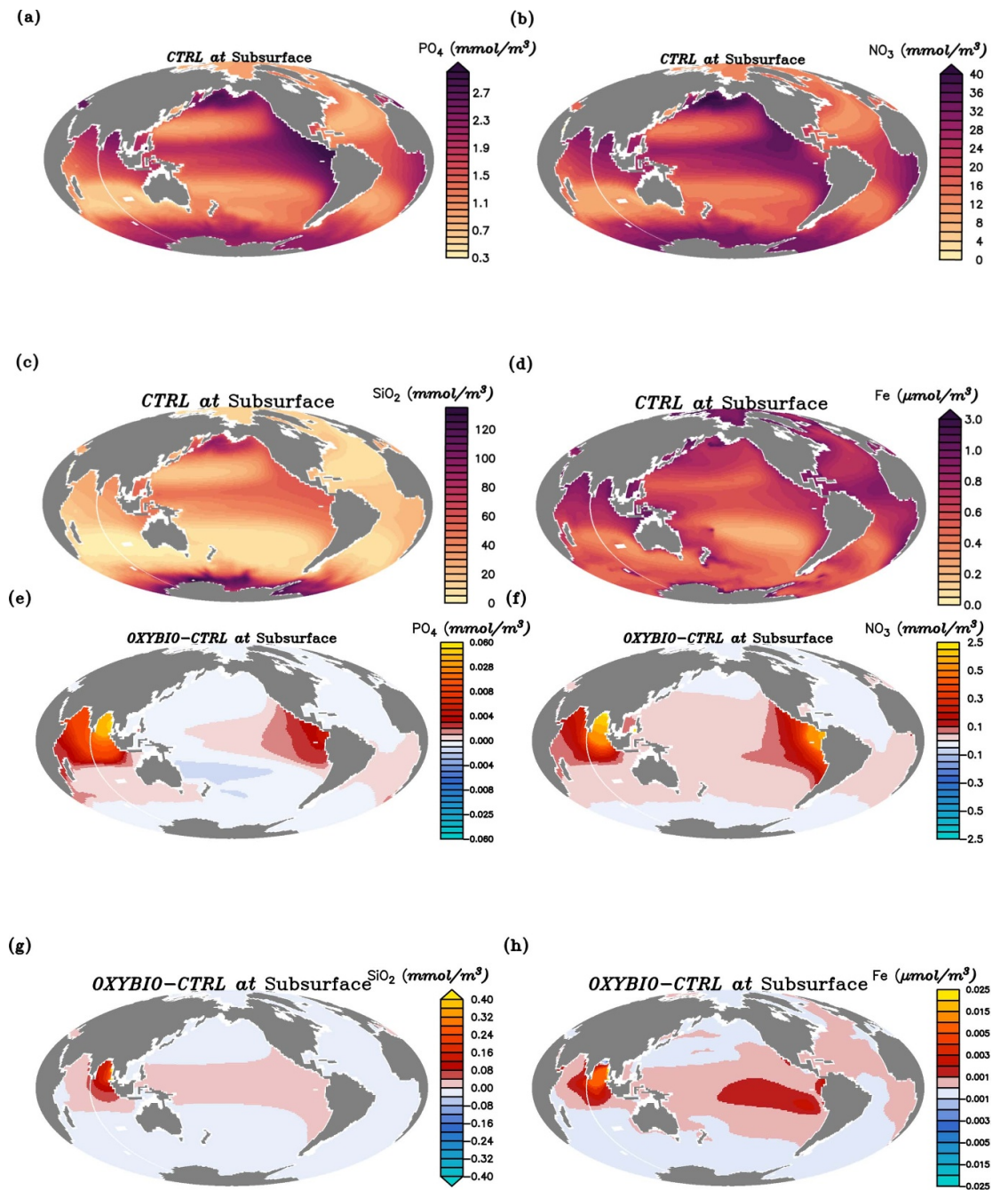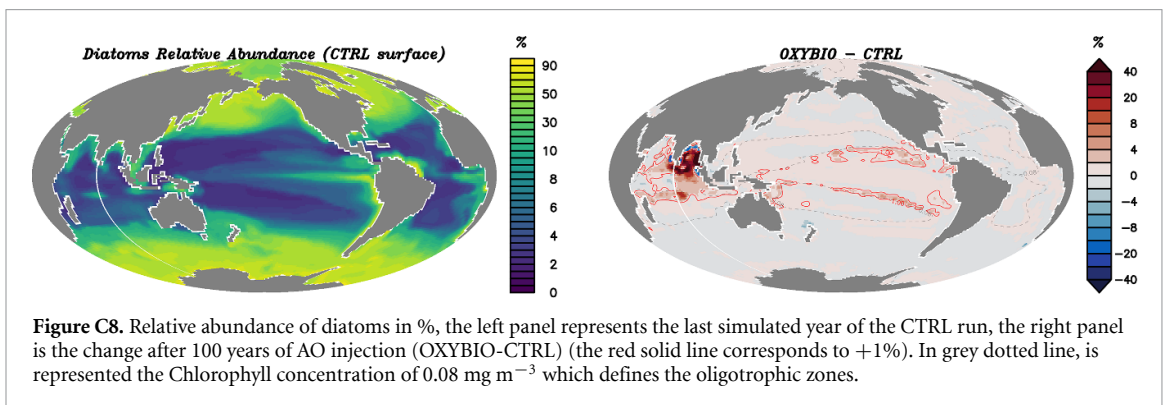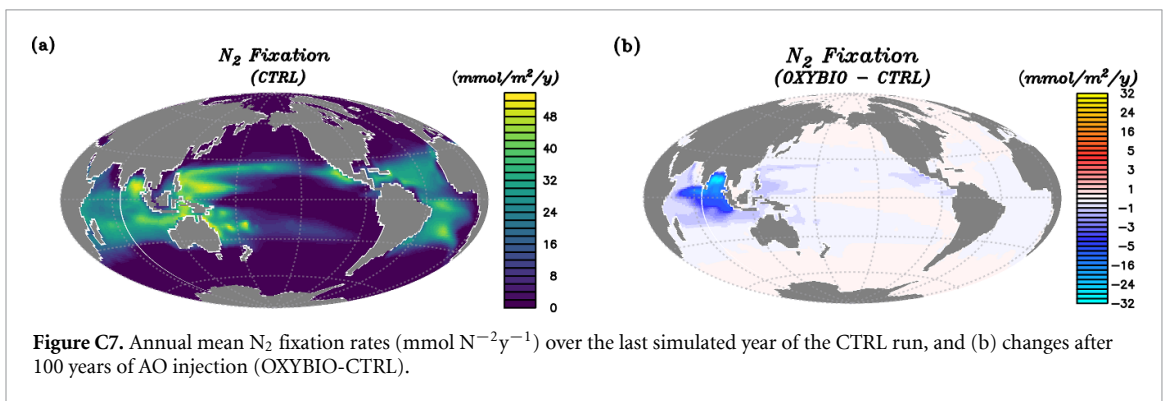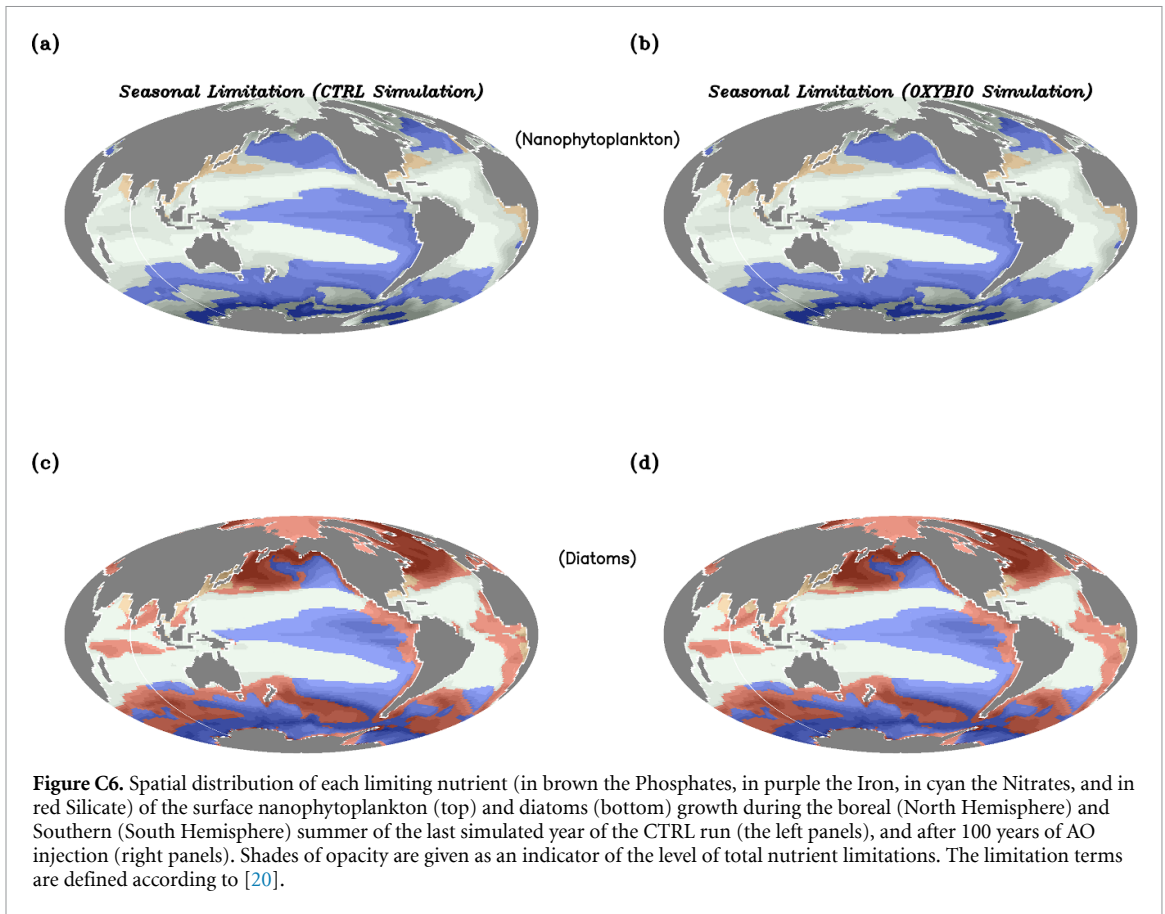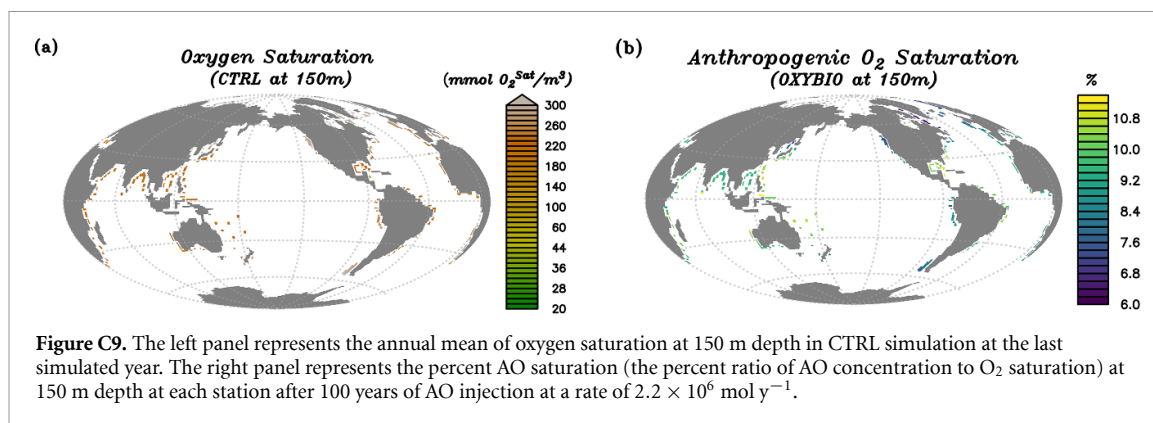
(a)

(b)

Seasonal Limitation (CTRL Simulation)   Seasonal Limitation (OXYBIO Simulation)

(Nanophytoplankton)

(c)

(d)

(Diatoms)

Figure C6. Spatial distribution of each limiting nutrient (in brown the Phosphates, in purple the Iron, in cyan the Nitrates, and in red Silicate) of the surface nanophytoplankton (top) and diatoms (bottom) growth during the boreal (North Hemisphere) and Southern (South Hemisphere) summer of the last simulated year of the CTRL run (the left panels), and after 100 years of AO injection (right panels). Shades of opacity are given as an indicator of the level of total nutrient limitations. The limitation terms are defined according to [20].

(a)

N_2 *Fixation*
(CTRL)   *(mmol/m²/y)*

(b)

N_2 *Fixation*
(OXYBIO − CTRL)   *(mmol/m²/y)*

Figure C7. Annual mean N_2 fixation rates (mmol $N^{-2}y^{-1}$) over the last simulated year of the CTRL run, and (b) changes after 100 years of AO injection (OXYBIO-CTRL).

Diatoms Relative Abundance (CTRL surface)   %   *OXYBIO − CTRL*   %

Figure C8. Relative abundance of diatoms in %, the left panel represents the last simulated year of the CTRL run, the right panel is the change after 100 years of AO injection (OXYBIO-CTRL) (the red solid line corresponds to +1%). In grey dotted line, is represented the Chlorophyll concentration of 0.08 mg m^{-3} which defines the oligotrophic zones.

Figure C9. The left panel represents the annual mean of oxygen saturation at 150 m depth in CTRL simulation at the last simulated year. The right panel represents the percent AO saturation (the percent ratio of AO concentration to O_2 saturation) at 150 m depth at each station after 100 years of AO injection at a rate of 2.2×10^6 mol y^{-1}.

ORCID iDs

Houda Beghoura https://orcid.org/0000-0001-6015-6355

Filippa Fransner https://orcid.org/0000-0001-8280-4018

Pierre-Amaël Auger https://orcid.org/0000-0001-7644-4087

References

[1] Feng E Y, Su B and Oschlies A 2020 Geoengineered ocean vertical water exchange can accelerate global deoxygenation *Geophys. Res. Lett.* **47** e2020GL088263

[2] Bopp L *et al* 2013 Multiple stressors of ocean ecosystems in the 21st century: projections with CMIP5 models *Biogeosciences* **10** 6225–45

[3] Cocco V *et al* 2013 Climate of the past geoscientific instrumentation methods and data systems oxygen and indicators of stress for marine life in multi-model global warming projections *Biogeosciences* **10** 1849–68

[4] Bograd S J, Castro C G, Di Lorenzo E, Palacios D M, Bailey H, Gilly W and Chavez F P 2008 Oxygen declines and the shoaling of the hypoxic boundary in the California current *Geophys. Res. Lett.* **35** L12607

[5] Deutsch C, Brix H, Ito T, Frenzel H and Thompson L A 2011 Climate-forced variability of ocean hypoxia *Science* **333** 336–9

[6] Stramma L, Johnson G C, Sprintall J and Mohrholz V 2008 Expanding oxygen-minimum zones in the tropical oceans *Science* **320** 655–8

[7] Stramma L , Prince E D, Schmidtko S, Luo J, Hoolihan J P, Visbeck M, Wallace D W R, Brandt P and Körtzinger A 2012 Expansion of oxygen minimum zones may reduce available habitat for tropical pelagic fishes *Nat. Clim. Change* **2** 33–37

[8] Schmidtko S, Stramma L and Visbeck M 2017 Decline in global oceanic oxygen content during the past five decades *Nature* **542** 335–9

[9] Bindoff N L *et al* 2022 Changing Ocean, Marine Ecosystems and Dependent Communities *The Ocean and Cryosphere in a Changing Climate* (Cambridge: Cambridge University Press) pp 447–588

[10] Keeling R F, Körtzinger A and Gruber N 2010 Ocean deoxygenation in a warming world *Ann. Rev. Mar. Sci.* **2** 199–229

[11] Kwiatkowski L *et al* 2020 Twenty-first century ocean warming, acidification, deoxygenation and upper-ocean nutrient and primary production decline from CMIP6 model projections *Biogeosciences* **17** 3439–70

[12] Sampaio E, Santos C, Rosa I C, Ferreira V, Pörtner H-O, Duarte C M, Levin L A and Rosa R 2021 Impacts of hypoxic events surpass those of future ocean warming and acidification *Nat. Ecol. Evol.* **5** 311–21

[13] Gruber N 2004 The dynamics of the marine nitrogen cycle and its influence on atmospheric CO2 variations *The Ocean Carbon Cycle and Climate* (Dordrecht: Springer) pp 97–148

[14] Breitburg D *et al* 2018 Declining oxygen in the global ocean and coastal waters *Science* **359** eaam7240

[15] Wagner K J 2019 Preface: advances in hypolimnetic oxygenation *Lake Reserv. Manage.* **35** 225–8

[16] Conley D J, Bonsdorff E, Carstensen J, Destouni G, Gustafsson B G, Hansson L-A, Rabalais N N, Voss M and Zillén L 2009 Tackling hypoxia in the baltic sea: is engineering a solution? *Environ. Sci. Technol.* **43** 3407–11

[17] Stigebrandt A *et al* 2015 An experiment with forced oxygenation of the deepwater of the anoxic by Fjord, western sweden *AMBIO* **44** 42–54

[18] Bhandari R, Trudewind C A and Zapp P 2014 Life cycle assessment of hydrogen production via electrolysis - a review *J. Cleaner Prod.* **85** 151–63

[19] Madec G 2015 NEMO ocean engine Gurvan Madec, and the NEMO team

[20] Aumont O, Ethé C, Tagliabue A, Bopp L and Gehlen M 2015 PISCES-v2: an ocean biogeochemical model for carbon and ecosystem studies *Geosci. Model Dev.* **8** 2465–513

[21] Wanninkhof R 2014 Relationship between wind speed and gas exchange over the ocean revisited *Limnol. Oceanogr.: Methods* **12** 351–62

[22] Körtzinger A, Hedges J I and Quay P D 2001 Redfield ratios revisited: removing the biasing effect of anthropogenic CO_2 *Limnol. Oceanogr.* **46** 964–70

[23] Lipschultz F, Wofsy S C, Ward B B, Codispoti L A, Friedrich G and Elkins J W 1990 Bacterial transformations of inorganic nitrogen in the oxygen-deficient waters of the eastern tropical South Pacific Ocean *Deep Sea Res.* A **37** 1513–41

[24] Cabré A, Marinov I, Bernardello R and Bianchi D 2015 Oxygen minimum zones in the tropical Pacific across CMIP5 models: mean state differences and climate change trends *Biogeosciences* **12** 5429–54

[25] Bao Y and Li Y 2016 Simulations of dissolved oxygen concentration in CMIP5 Earth system models *Acta Oceanol. Sin.* **35** 28–37

[26] Garcia H E, Locarnini R A, Boyer T P, Antonov J I, Baranova O K, Zweng M M and Johnson D R 2010 *World Ocean Atlas 2009, Volume 4: Nutrients (Phosphate, Nitrate, Silicate), Noaa Atlas Nesdis* 71st edn (Washington, DC: US Government Printing Office) p 398

[27] International Energy Agency (IEA) 2019 Offshore wind outlook 2019: world energy outlook special report (available at: www.iea.org/t&c/)

[28] LHYFE production units (www.lhyfe.com/our-production-units/)

[29] Saint-Drenan Y-M, Besseau R, Jansen M, Staffell I, Troccoli A, Dubus L, Schmidt J, Gruber K, Simões S G and Heier S 2020 A parametric model for wind turbine power

curves incorporating environmental conditions *Renew.
Energy* **157** 754–68

[30] United Nations. World Population Prospects - Population
Division - United Nations (https://population.un.org/wpp/)

[31] Paulmier A and Ruiz-Pino D 2008 Oxygen minimum zones
(OMZs) in the modern ocean *Prog. Oceanogr.* **80** 113–28

[32] Chen L, Dong X, Wang Y and Xia Y 2016 Separating
hydrogen and oxygen evolution in alkaline water electrolysis
using nickel hydroxide *Nat. Commun.* **7** 11741

[33] Bianchi D, Galbraith E D, Carozza D A, Mislan K A S and
Stock C A 2013 Intensification of open-ocean oxygen
depletion by vertically migrating animals *Nat. Geosci.*
6 545–8

[34] Chinni V and Singh S K 2022 Dissolved iron cycling in the
Arabian Sea and sub-tropical gyre region of the Indian
Ocean *Geochim. Cosmochim. Acta* **317** 325–48

[35] Twining B S, Nodder S D, King A L, Hutchins D A,
LeCleir G R, DeBruyn J M, Maas E W, Vogt S, Wilhelm S W
and Boyd P W 2014 Differential remineralization of major
and trace elements in sinking diatoms *Limnol. Oceanogr.*
59 689–704

[36] Devries T and Deutsch C 2014 Large-scale variations in the
stoichiometry of marine organic matter respiration *Nat.
Geosci.* **7** 890–4

[37] Long M C, Deutsch C and Ito T 2016 Finding forced trends
in oceanic oxygen *Glob. Biogeochem. Cycles* **30** 381–97

[38] Rixen T , Cowie G, Gaye B, Goes J, do Rosário Gomes H,
Hood R R, Lachkar Z, Schmidt H, Segschneider J and
Singh A 2020 Reviews and syntheses: present, past and future
of the oxygen minimum zone in the northern Indian Ocean
Biogeosciences **17** 6051–80

[39] de Baar H J W 1994 von Liebig's law of the minimum and
plankton ecology (1899-1991) *Prog. Oceanogr.* **33** 347–86

[40] Landolfi A, Dietze H, Koeve W and Oschlies A 2013
Overlooked runaway feedback in the marine nitrogen cycle:
the vicious cycle *Biogeosciences* **10** 1351–63

[41] Kelly T B , Knapp A N, Landry M R, Selph K E,
Shropshire T A, Thomas R K and Stukel M R 2021 Lateral
advection supports nitrogen export in the oligotrophic
open-ocean Gulf of Mexico *Nat. Commun.* **12** 3325

[42] Cullen J J, Franks P J S, Karl D M and Longhurst A 2002
Physical influences on marine ecosystem dynamics *The Sea:
Biological-Physical Interactions in the Ocean* vol 12, ed A
R Robinson, J J McCarthy and B J Rothschild (New York:
Wiley) ch 8, pp 297–336

[43] Brix H, Gruber N, Karl D M and Bates N R 2006 On the
relationships between primary, net community and export
production in subtropical gyres *Deep Sea Res.* II **53** 698–717

[44] Alvain S, Moulin C, Dandonneau Y and Loisel H 2008
Seasonal distribution and succession of dominant
phytoplankton groups in the global ocean: a satellite view
Glob. Biogeochem. Cycles **22**

[45] Sarthou G, Vincent D, Christaki U, Obernosterer I,
Timmermans K R and Brussaard C P D 2008 The fate of
biogenic iron during a phytoplankton bloom induced by
natural fertilisation: impact of copepod grazing *Deep Sea
Research* II **55** 734–51

[46] Coale K H *et al* 2004 Southern Ocean iron enrichment
experiment: carbon cycling in high- and low-Si waters
Science **304** 408–14

[47] Boyd P W *et al* 2004 The decline and fate of an iron-induced
subarctic phytoplankton bloom *Nature* **428** 549–53

[48] Boyd P W *et al* 2000 A mesoscale phytoplankton bloom in
the polar Southern Ocean stimulated by iron fertilization
Nature **407** 695–702

[49] Legendre L and LeFèvre J 1991 From individual plankton
cells to pelagic marine ecosystems and to global
biogeochemical cycles *Particle Analysis in Oceanography*
(Berlin: Springer) pp 261–300

[50] Aumont O and Bopp L 2006 Globalizing results from ocean
in situ iron fertilization studies *Glob. Biogeochem. Cycles*
20 GB2017

[51] Jenkins W J 1987 3 H and 3 He in the beta triangle:
observations of gyre ventilation and oxygen utilization rates
J. Phys. Oceanogr. **17** 763–83

[52] Martin J H, Knauer G A, Karl D M and Broenkow W W 1987
VERTEX: carbon cycling in the northeast Pacific *Deep Sea
Res.* A **34** 267–85

[53] Feely R A, Sabine C L, Schlitzer R, Bullister J L, Mecking S
and Greeley D 2004 Oxygen utilizatiuon and organic carbon
remineralization in the upper water column of the Pacific
Ocean *J. Oceanogr.* **60** 45–52

[54] Karstensen J, Stramma L and Visbeck M 2008 Oxygen
minimum zones in the eastern tropical Atlantic and Pacific
Oceans *Prog. Oceanogr.* **77** 331–50

[55] Lévy M, Resplandy L, Palter J B, Couespel D and Lachkar Z
2022 The crucial contribution of mixing to present and
future ocean oxygen distribution *Ocean Mixing*
(Amsterdam: Elsevier) pp 329–44

[56] Resplandy L, Lévy M, Bopp L, Echevin V, Pous S, Sarma V V
S S and Kumar D 2012 Controlling factors of the oxygen
balance in the Arabian Sea's OMZ *Biogeosciences* **9** 5095–109

[57] Lachkar Z, Smith S, Lévy M and Pauluis O 2016 Eddies
reduce denitrification and compress habitats in the Arabian
Sea *Geophys. Res. Lett.* **43** 9148–56

[58] Gilly W F, Beman J M, Litvin S Y and Robison B H 2013
Oceanographic and biological effects of shoaling of the
oxygen minimum zone *Ann. Rev. Mar. Sci.* **5** 393–420

[59] Chavez F P, Messié M and Pennington J T 2011 Marine
primary production in relation to climate variability and
change *Ann. Rev. Mar. Sci.* **3** 227–60

[60] Bertrand A , Chaigneau A, Peraltilla S, Ledesma J, Graco M,
Monetti F and Chavez F P 2011 Oxygen: a fundamental
property regulating pelagic ecosystem structure in the
Coastal Southeastern Tropical Pacific *PLoS ONE* **6** e29558

[61] Tagliabue A , Kwiatkowski L, Bopp L, Butenschön M,
Cheung W, Lengaigne M and Vialard J 2021 Persistent
uncertainties in ocean net primary production climate
change projections at regional scales raise challenges for
assessing impacts on ecosystem services *Frontiers Clim.*
3 149

[62] Tréguer P *et al* 2018 Influence of diatom diversity
on the ocean biological carbon pump *Nat. Geosci.*
11 27–37

[63] Bristow L A *et al* 2017 N2 production rates limited by nitrite
availability in the Bay of Bengal oxygen minimum zone *Nat.
Geosci.* **10** 24–29

[64] Berman-Frank I *et al* 2008 Feedbacks between the nitrogen,
carbon and oxygen cycles *Nitrogen in the Marine
Environment* (Amsterdam: Elsevier) pp 1537–63

[65] Dutheil C, Aumont O, Gorgués T, Lorrain A, Bonnet S,
Rodier M, Dupouy C, Shiozaki T and Menkes C 2018
Modelling N2 fixation related to trichodesmium sp.: driving
processes and impacts on primary production in the tropical
Pacific Ocean *Biogeosciences* **15** 4333–52

[66] Löptien U and Dietze H 2017 Effects of parameter
indeterminacy in pelagic biogeochemical modules of earth
system models on projections into a warming future: the
scale of the problem *Glob. Biogeochem Cycles* **31** 1155–72

[67] Bopp L, Resplandy L, Untersee A, Le Mezo P and
Kageyama M 2017 Ocean (de)oxygenation from the last
glacial maximum to the twenty-first century: insights from
earth system models *Phil. Trans. R. Soc.* A **375** 20160323

[68] Dietze H and Löptien U 2021 Retracing hypoxia
in Eckernförde bight (Baltic Sea) *Biogeosciences*
18 4243–64

[69] Beghoura H *et al* 2022 Contrasting responses of the Ocean's
Oxygen Minimum Zones to artificial re-oxygenation
(https://doi.org/10.5281/zenodo.7377077)

[70] Garcia H E *et al* 2019 *World Ocean Atlas 2018, Volume 3:
Dissolved Oxygen, Apparent Oxygen Utilization, and
Dissolved Oxygen Saturation* 83, 38pp (NOAA Atlas NESDIS)
(available at: www.nodc.noaa.gov/OC5/woa18/pubwoa18.
html)